

Safe Operation of Combined Cycle Gas Turbine and Gas Engine Systems using Hydrogen Rich Fuels

Wayne Rattigan, Senior Scientist, Science Division, Health and Safety Executive, Harpur Hill, Buxton, Derbyshire, UK.

The High Hydrogen project commissioned by the Energy Technologies Institute was completed in 2019. The project was led by the Science Division of the Health and Safety Executive and delivered in collaboration with Imperial College and Scitek Consultants Ltd.
The overall objective of the project was to model at reduced scale the consequences of a flameout in a full size combined cycle gas turbine (or gas engine) when running on hydrogen or on fuels containing a large amount of hydrogen, such as syngas. In so doing the intention was to provide data sets that could be used to aid the understanding of the physical processes involved, identify the safe operational boundaries, and thereby aid the determination of cost effective design solutions for the future use of such fuels.
The purpose-built facility was designed and built by the Science Division of the HSE to meet the experimental testing requirements of the project. The facility incorporated a Rolls-Royce Viper 301 Jet Engine (Gas Turbine) converted to run on butane. This provided a hot exhaust stream into which make-up oxygen and the test gas mixture were injected and then ignited. The resulting flame front travelled along a circular duct before entering an expansion chamber and then a model heat exchanger, which consisted of fifteen rows of solid finned tubing giving a blockage ratio of 48% per row. The increased turbulence created in this region accelerated the flame front, which in some instances generated unacceptably high pressures within the overall system. The system vented through a vertical opening downstream of the heat exchanger. There were in excess of fifty sensors strategically placed along the system to measure dynamic pressures, oxygen concentrations, flame front positions and the flame speeds.
This paper describes the experimental test rig, its design and operation, together with the range and concentrations of fuels tested as defined by their equivalence ratios (EQR's) and mixture concentrations. An analysis of the data collected is presented together with an assessment of the test results.

Keywords: Hydrogen; combined-cycle gas turbine; combined-cycle gas engine; detonation; flameout; deflagration;

Introduction

This paper describes the experimental study carried out within a reduced scale model of a combined cycle gas turbine (CCGT) complete with a model heat recovery steam generator (HRSG), designed, built and operated by the Science Division of the Health & Safety Executive (HSE) and its collaborators on behalf of the ETI.
The purpose of the study was to simulate the conditions and consequences within the HRSG, arising from a gas turbine flameout condition. This was achieved by carrying out measurements following ignition of flammable gas mixtures in air, when injected into the hot vitiated exhaust stream from a Rolls-Royce Viper jet engine. Of particular interest from a safety perspective was the peak pressure which could result under different mixture conditions. The fuel gases studied were 100% hydrogen, 100% methane or binary mixtures of hydrogen with methane or hydrogen with carbon monoxide.

Background

A database of 343 gas turbine related incidents was developed by HSL based on records from 1981 to 2004 and an analysis of the database was published by Santon (2005).
This analysis shows that there were 16 incidents of explosions in gas turbine exhaust systems within the records and of these, there are 9 records of explosions in exhaust systems in UK offshore locations, where the average number of turbines in use is known to have been 554. From this data it can be estimated that the risk of an explosion in an exhaust system was 1 in 1400 per turbine per year. A large body of safety regulation and guidelines exist with relevance to this subject area and covering safe handling of hydrogen fuels (e.g. ISO-PDTR-15916, 2010, NASA-NSS-1740.16, 1997), explosion prevention and venting (e.g. BS-EN-1127, 2011, NFPA-68, 2008), safe design and operation of CCGT and gas engines (e.g. NFPA-85, 2011, IGEM3, 2006) and gas turbine operations (e.g. BS-ISO-21789, 2009). The current work breaks new ground in respect of the use of high hydrogen fuels within areas which previously used less reactive fuels.
Of particular interest therefore among operators and modellers are the prediction techniques for the calculation of overpressures resulting from explosions using such fuels, and examples of these have been formulated by a number of commercial vendors. These techniques are typically based on variants on moment closures with a prevalence of eddy-viscosity based methods. A number of these approaches have been reviewed by Arntzen et al. (Arntzen, 1995) following the completion of major EU projects aimed at procuring reference data in large-scale explosions. More sophisticated techniques have also been applied and evaluated in the context of explosion initiation in confined flows of direct relevance to the current study (Kuan, 2003).
Gamezo and co-workers have presented extensive studies of flows making more rapid transition to DDT. These studies have traditionally been focussed on strong initiation (e.g. via shock wave interactions), but more recently extended studies featuring strongly turbulent flows have also been considered (Gamezo, 2007).
The key challenge for all prediction methods can be found in the interaction of the chemistry of a particular fuel mixture with flow and a sufficiently accurate description of generation of turbulence through interactions with obstructions and

boundary layers. To date, only a very limited number of studies have sought to clarify this link, for example through the application of time-resolved laser diagnostics for the quantification of flow statistics, a good example being the work of Lindstedt and co-workers (Lindstedt 2001).
The reported work was aimed at generating practical data for operators and thus provide a detailed evidence base for, and advance the state-of-the-art in, the safe and efficient operation of high hydrogen gas mixtures for energy production. It will help to identify the bounds of safe design and operation of proposed high hydrogen systems to avoid unpredicted hazardous outcomes (limits of flammability, ignition and significant overpressure potential, including DDT) in the exhaust systems of a range of combined heat and power (CHP) and CCGT applications. It will allow existing systems to be operated with more confidence within their bounds of safety in order to increase energy production and avoid unnecessary trips (for example, enabling gas engines to run at higher fuel/air ratios, or operating CCGT systems with higher trip set-points). The work also provides a substantial and detailed database of results for those involved in modelling and reproducing the time resolved flame and pressure behaviour.

Experimental Facility

The overall experimental facility comprised the following major components: jet engine, experimental rig, gas delivery system, computer operating systems for the gas delivery and the jet engine and data acquisition.

Jet Engine

A Rolls-Royce Viper type 301 jet engine, converted to run on liquid butane and fed from an 8000 litre tank using a low pressure circulating pump and a high pressure fuel pump via associated pipework and control valves, was used to provide a hot vitiated air stream into the circular duct. The jet engine was isolated externally from the main experimental rig by a thick steel plate and was housed in a concrete block structure (Figure 1) as a safety precaution.

Figure 1. Rolls-Royce Viper Type 301 jet engine modified to run on liquid butane

The jet engine was capable of producing mass flow rates between 5 kg/s and 15 kg/s as a function of the engine rpm. However, the mass flow into the test rig was modulated via a diverter section. This allowed exhaust from the jet engine to be spilled to atmosphere and in combination with a changeable orifice plate at the entrance to the test duct gave actual velocities into the duct of between 50 m/s and 90 m/s at a nominal mass flow of around 11 kg/s. Changing the orifice plate, in combination with altering the engine rpm, allowed the nominal temperature within the duct to be controlled within the range of 320 °C to 550 °C.

Experimental Test Rig

The test rig is intended to mimic the arrangement in a full scale combined cycle gas turbine. Figure 2 identifies the main components. The exhaust from the jet engine enters into the test rig via a transition section. The test rig comprises a 0.6 m diameter test duct, comprising four 3 metre long sections, beginning with transition and diverter sections, and a removable turbulence generator. Attached to the end of the duct is an expansion section, a tube bank, end plate and an exit stack, all combining to form a scaled model of an actual HRSG. The heat exchanger and sections downstream (HR4, HR5 and HR6) are 6.4 m in length, 2.8 m in height and 1.4 m wide. Note that the circular duct section does not exist in an actual gas turbine exhaust system and its presence may add to the exhaust turbulence around the tube bundle region.

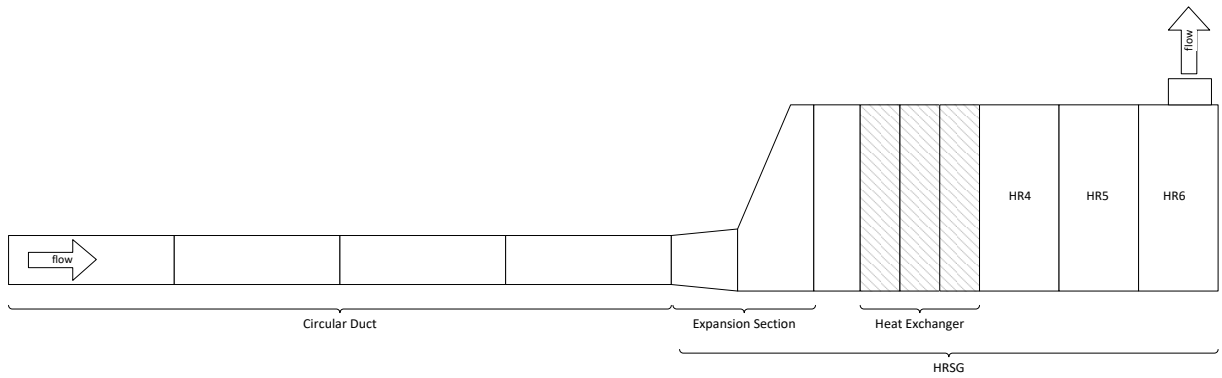

Figure 2. A simple schematic (not to scale) showing main components of the test rig: the circular duct; the expansion section; the heat exchanger and empty downstream sections HR4, HR5 and HR6, and the exhaust duct.

An image of the HRSG section during construction is shown in Figure 3.

Figure 3. Image of HRSG under construction, showing open exit from circular duct. The first 3 sections of the HRSG and the 3 sections of the heat exchanger are shown.

Fuel and Oxygen Supply Systems (Gas Delivery)

The gases were injected into the rig via two independent systems, one for the oxygen and one for the fuel gases. Both systems incorporated twin storage cylinders giving a capacity of 500 litres of gas stored at pressures up to 230 bar. Where binary or ternary mixtures of hydrogen, methane and carbon monoxide were being tested the storage cylinders could be charged with the individual gases using the partial pressure method and could then be recirculated using the gas booster pump, ensuring good mixing. Gases were charged into the experimental rig via a flow control system comprising a pressure regulator, Coriolis flow meter and flow control valve. The oxygen gas delivery system was capable of injecting oxygen sufficient to restore levels to 21% in the exhaust stream when operating at up to 15 kg/s, equivalent to a maximum oxygen mass flow rate of 1.12 kg/s. The oxygen concentration within the engine exhaust stream was measured using a Servomex Mini MP 5200 and the required mass of oxygen to return this level to 21% was calculated for the given engine mass flow.
The fuel gas delivery system, comprising mixtures of hydrogen, methane, and carbon monoxide, or each gas individually, was capable of delivering up to maximum mass flow rates of 0.2 kg/s, 1.57 kg/s and 2.74 kg/s for the three gases respectively. The system was capable of injecting fuel mixtures up to 15% by volume at the maximum mass flow rates. Figure 4 shows the radially arranged injection tube system designed to optimise mixing within a short distance.

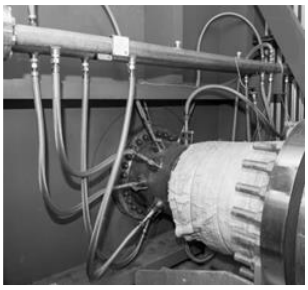

Figure 4: Radially arranged fuel and oxygen injection tube system.

Sensors

The rig was populated with an array of sensors to capture the progress of the flame front and pressure pulse within duct and HRSG. To this end the sensors comprised thermocouples, pressure transducers, ionisation probes (IPs) and optical probes (OPs). Flame progress was also captured by the use of two high-speed video cameras located upstream of the heat exchanger above the expansion section and on the end plate looking back toward the heat exchanger.
Detection of the flame by means of flame ionisation and optical emission techniques have provided complementary measurements in that the optical sensors observed a line of sight across the diameter, whilst the ionisation sensors were point measurement devices located on the side walls and would only detect when a flame was present locally. Generally the optical sensors captured the flame passage under most conditions, whilst the ionisation sensors were more intermittent in their detection, with weak flame events often being unrecorded, either due to their inherent weakness or their absence in the wall region. A number of high speed photography tests have confirmed the variability in flame behaviour under different conditions of mixture and equivalence ratio. The pressure detection often showed complex behaviour arising from the different sensor locations and the changing flame speed behaviour within the duct due to the distribution of obstacles. In many cases the peak pressure was of short duration and followed by longer duration, lower pressure components. This may have implications for the real impact of pressure pulses on the containing structures.

Control and Data Acquisition System

The jet engine and gas delivery control were operated by two independent computer systems. The end plate and exit stack shown in Figure 2 were attached for all of the tests discussed in this paper. Pitot-static probe measurements of the velocity and temperature profiles across the circular duct were made prior to each test to establish exhaust mass flows.
Measurements of both the static pressures, using Kulite sensors, and temperatures using type K thermocouples were made along the duct and within the HRSG during testing. It is noted that thermocouple response times were to slow to capture flame progress following ignition but provided the starting conditions for each test.
The data logging and processing system captured data at a resolution of 16-bits or better and the maximum sampling rates were up to 1 MHz, but for the tests describes the data acquisition rate was 100 kHz.

Results

Definition of Equivalence Ratio (EQR)

The definition of equivalence ratio (EQR) used throughout the work should be noted, since this is based on the mole fraction ratio of the fuel in the fuel/air mixture rather than the more commonly used mole ratio of fuel and air.

Defining the following terms:- M_F = moles of fuel, M_A = moles of air, then the molar ratio of fuel and air is: M_F / M_A.

Under stoichiometric conditions, the stoichiometric molar fuel/air ratio is S_{mr}, where S_{mr} = M_F / M_{As} and where M_{As} is the stoichiometric moles of air corresponding to M_F moles of fuel.

For an arbitrary number of fuel moles M_F' and air moles M_A', the equivalence ratio EQR_{mr}, based on fuel and air mole ratios is then:

EQR_{mr} = M_F' / M_A' x M_{As} / M_F i.e. M_F' / M_A' x 1 / S_{mr}

This formula would correspond to the commonly used definition of EQR. In the present work mole fractions are used to represent the EQR parameter.

The stoichiometric mole fraction fuel air ratio, S_{mfr}, then becomes :- $S_{mfr} = \frac{M_F}{M_F + M_{As}}$

where M_{As} corresponds to the stoichiometric moles of air corresponding to M_F moles of fuel.

The equivalence ratio used in the present work is then defined as EQR_{mfr}, where

$$EQR_{mfr} = \frac{M'_F}{M'_F + M'_A} \cdot \frac{1}{S_{mfr}}$$

and where M_F' and M_A' are the actual mole quantities used in a test.

It can readily be shown that a conversion between the above two definitions of EQR can be derived, and this relation is the following:

$$EQR_{mr} = EQR_{mfr} \cdot \frac{(1 - S_{mfr})}{(1 - EQR_{mfr} \cdot S_{mfr})}$$

The EQR_{mfr} values are always provided for each test and the stoichiometric mole fraction ratios (S_{mfr}) are shown in Table 1 for the mixtures used in the test series.

Table 1. Stoichiometric mole fractions for the mixtures used in the test series.

Fuel mixture	S_{mfr}
100% CH_4	0.095
60% H_2/40% CH_4	0.1603
40% H_2/ 60% CH_4	0.1304
CO	0.2957
40% H_2/ 60% CO	0.2957
60% H_2/ 40% CO	0.2957
H_2	0.2957
40% H_2/ 25% CH_4/ 35% CO	0.1935

General Behaviour of flame and pressure pulses following ignition

In total there were 76 tests carried out in the full experimental rig and the data is therefore extensive. The main features can be depicted in a number of ways to aid understanding. In all cases where a successful ignition occurred (i.e., did not auto-ignite) a flame-front travelled down the duct at a velocity dependent upon the test conditions, its progress being tracked by the optical sensors located in the duct. Because of the asymmetry of the expansion section geometry, the unburned gas flow induced by the flame produces a wall jet on the bottom of the channel. The flame-front travels faster in this high speed flow near the bottom of the expansion section and thus reaches the tube bank first. The key feature is the influence of the tube bank in generating flame acceleration through turbulence, and the associated pressure wave. The pressure wave travels through the tube bank at a low level before spreading upwards and sideways in the first section of the HRSG after the tube bank. Before the flame arrives at the tube bundle there is a pressure gradient developed in the tube bundle that is associated with the flow restriction. Consequently the flame enters the tube bundle in which there is an already existing pressure gradient. The flame velocity in the expansion section is not sufficiently high to have a significant pressure wave associated with it. The combustion and pressure generation in the tube bundle is rather complex where a pressure "pulse" develops ahead of the flame as a result of the acceleration process. The flow immediately after the tube bundle is highly turbulent due to the turbulence convected downstream from the tubes. Once the flame reaches this turbulent region rapid combustion of the gas can lead to further pressure pulse generation, which amplifies the pressure pulse (associated with the flame acceleration) that leaves the tube bundle. The speed at which this process occurs is dependent upon the nature and strength of the fuel mixture being tested. The pressure pulse travels along the length of the last three HR sections at the relevant sound speed before being reflected backwards off the end wall. There is venting of the combusted gas out through the stack, at the end of the HRSG, which reduces the strength of the reflected pressure wave.

A useful starting point to illustrate these features of the combustion event following ignition of the mixture are the following graphs.

Figure 5 shows three of the main events following ignition, which are characteristic of the whole series of test results. The upper trace shows the flame ionisation signal as flame passes the exit of the circular duct (IP0). This flame progresses through the expansion section into the heat exchanger (HE) tube bank where it is identified as shown on the middle trace, by IP9 located on the side of the middle panel.

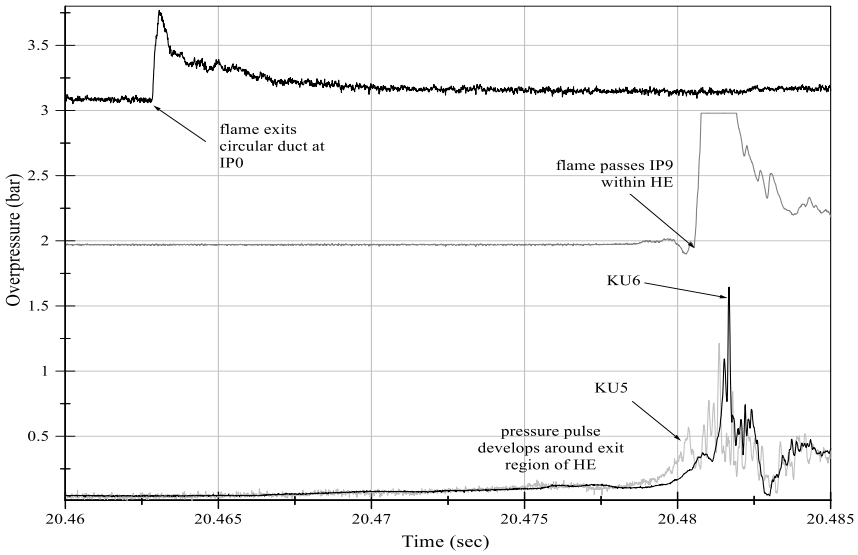

Figure 5. Relationship between flame progress through circular duct and HRSG system and associated pressure generation

The flame accelerates through turbulence generation within the tube bank into the region immediately downstream of the tube bank in HR4. This is a turbulent flow region, where the main combustion driven pressure wave is generated. Since the turbulent region is finite and assumed to be of the order of 1m in length, (based on a typical pulse width of 5msec and flame speed in HR4 of around 100 - 200m/s), the pressure generated in this region cannot be maintained as the flame progresses further along the exhaust duct (HR4-HR6) due to a reduced rate of combustion. This results in a pressure pulse of finite width as shown in the KU5 and KU6 traces of Figure 5.

The time width of the pulse is illustrated by the case shown in Figure 6. An initial pressure pulse can be seen as recorded on Kulite 6 (KU6) of around 5 ms width and 0.64 barg in amplitude. In this same figure a second pulse can be seen around 16.6 ms later, on KU6, arising from a reflection off the downstream end plate of the HRSG. It is important to note that this initial source pressure pulse (at around 21.39 s) is the origin of subsequent pressure pulse behaviour within the whole system and that the evolution of this initial wave arises through normal propagation, reflection and pulse sharpening associated with regular shock behaviour. These fluid dynamic effects often result in the propagated wave being greater in amplitude than the original wave, even within the region where it first originated. Due to the importance of this initial pressure wave around the heat exchanger, it is given special attention, and subsequent plots of pressure vs EQR use this initial wave as the basis for comparison between different test conditions.

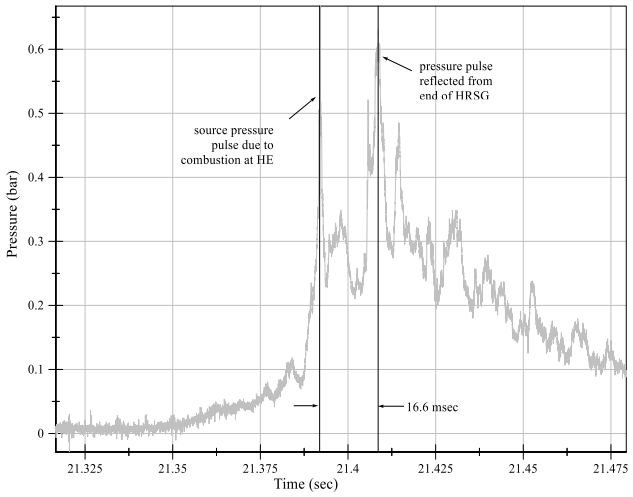

Figure 6. Typical pressure pulse profile immediately downstream of heat exchanger (Ku6) for a fast combustion event

Another pressure pulse feature observed, and illustrated in Figure 7 from Test 40 (100% H_2, EQR=0.54), is a series of short pressure pulses recorded just after the tube bundle by KU6. This is associated with more reactive mixture conditions, and is assumed to be a feature of the unsteady flow and highly turbulent region around the tube bank exit and immediately downstream of the tube bank. The time period of around 15 ms for the reflected wave to reach KU6 represents a velocity of around 600 m/s, the sound speed in the hot gas mixture through which it travels.

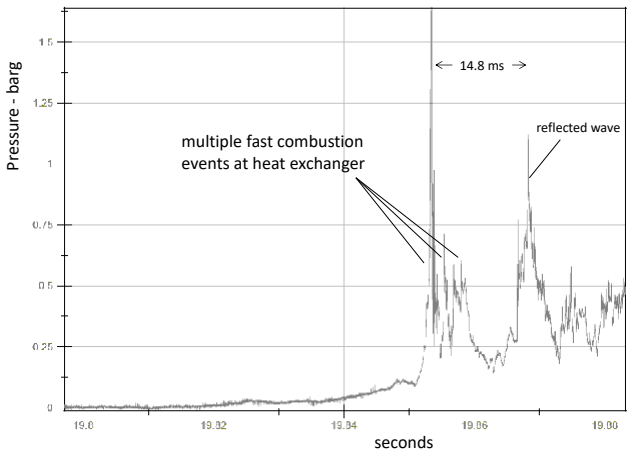

Figure 7 . Multiple fast combustion events at the heat exchanger

Figure 8 shows the relationships between the pressure measurements in the duct (KU1) and those downstream in the HRSG (KU7). In particular, the back pressure created by the flame-front as it leaves the duct and later the backwards travelling pressure pulse from the reflected pulse off the end wall coming back through the heat exchanger tube bank. As can be seen the transit time of the initial pressure pulse at 24.97ms travelling at sound speed back to the circular duct KU1 is 5.5ms.

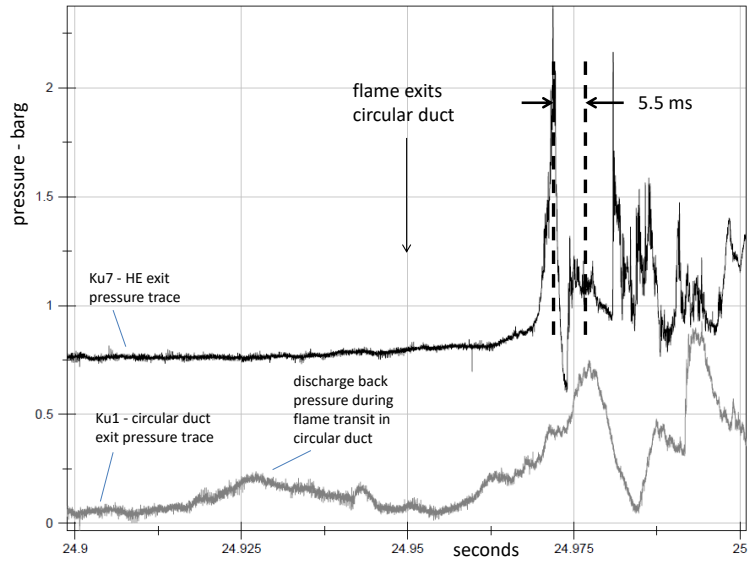

Figure 8. Pressure trace relationship between end of section 4 of HRSG and end of circular duct

The trace from KU7 illustrates the amplification of the initial pressure pulse (flame-front) as it emerges from the turbulent region immediately downstream of the tube bank, and also shows the delay before this pressure pulse reaches the upstream KU1 pressure sensor in the circular duct. This pressure pulse is lower in magnitude than the following wave that has been reflected from the end wall of the HRSG. The time point at which the flame leaves the circular duct (based on IP0) is also indicated.

The pressure front and flame front will ultimately emerge from the vertical chimney at the end of the HRSG, as shown in Figure 9 below, using a mixture of 60%CH_4/40%H_2 and an EQR of 0.7. The extent of the visible flame depends on the strength of the pressure wave, which itself is dependent upon the fuel composition and its' EQR.

Figure 9. Flame emerging from exhaust duct during a test with the end plate on

Results Data

The key feature of the ignition tests discussed above was the finite duration pressure pulse generated by the fast combustion within and immediately beyond the heat exchanger tubes. This pulse, of a few milliseconds duration, propagated through the

system at sound speed and was subject to the normal compressible flow behaviour associated with shock waves, e.g. sharpening, and attenuation. For this reason the peak pressures recorded at different parts of the system could have different amplitudes. Two pressures were of particular interest. These were the peak pressure immediately downstream of the heat exchanger, i.e. the 'source pressure', and the maximum pressure recorded during a test. The former provided insight into the combustion rate in the region of high turbulence whilst the latter indicated the potential hazard which could arise for a particular fuel and EQR tested. Tests were carried out with a range of exhaust temperatures, i.e. 550, 480 and 320 °C and in the results presented below for different fuels and EQR values, peak pressures are presented immediately after the heat exchanger and also the highest peak pressure recorded during a test. Importantly, this maximum pressure would often arise in the end-plate region where the pressure pulse underwent a transient doubling of pressure during the pulse reflection event.

The following tables and graphs show the peak and maximum pressures over a range of temperatures and EQR values for 100%H_2, 100%CH_4, 60%H_2/40%CH_4, 40%H_2/60%CH_4 and 60%CO/40%H_2.

Table 2. Results of experiments on 100% hydrogen

Eq. Ratio	Peak Pressure mbar	Initial Pressure after HE mbar	Nominal Temperature °C
0.470	621	390	550
0.510	1016	920	550
0.550	1971	1790	550
0.410	322	152	550
0.440	522	276	550
0.480	987	525	550
0.520	2196	710	480
0.480	1158	475	480
0.540	3115	1626	480
0.420	601	276	480
0.350	251	145	480
0.540	3430	1639	480
0.450	2833	1487	320
0.350	502	266	320
0.285	278	115	320

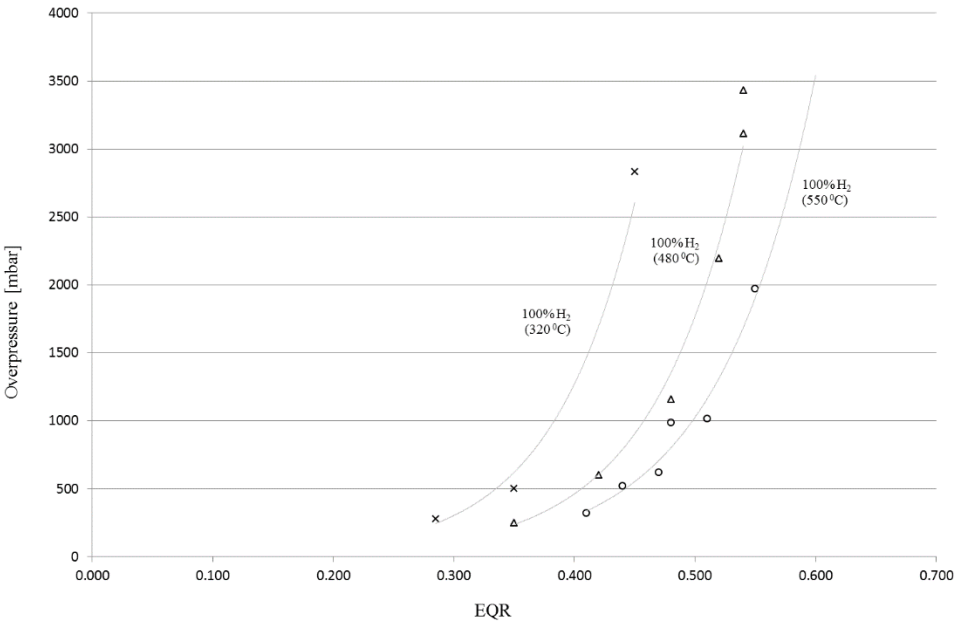

Figure 10. Peak pressure of explosion within the experimental rig plotted at different equivalence ratios for tests on 100% H_2 at nominal temperatures of 320 °C, 480 °C and 550 °C

Table 3. Results of experiments on 100% methane

Eq. Ratio	Peak Pressure mbar	Initial Pressure after HE mbar	Nominal Temperature °C
0.640	385	150	550
0.790	967	683	550
0.490	117	42	550
0.650	394	142	320
0.810	831	303	320
0.506	102	38	320

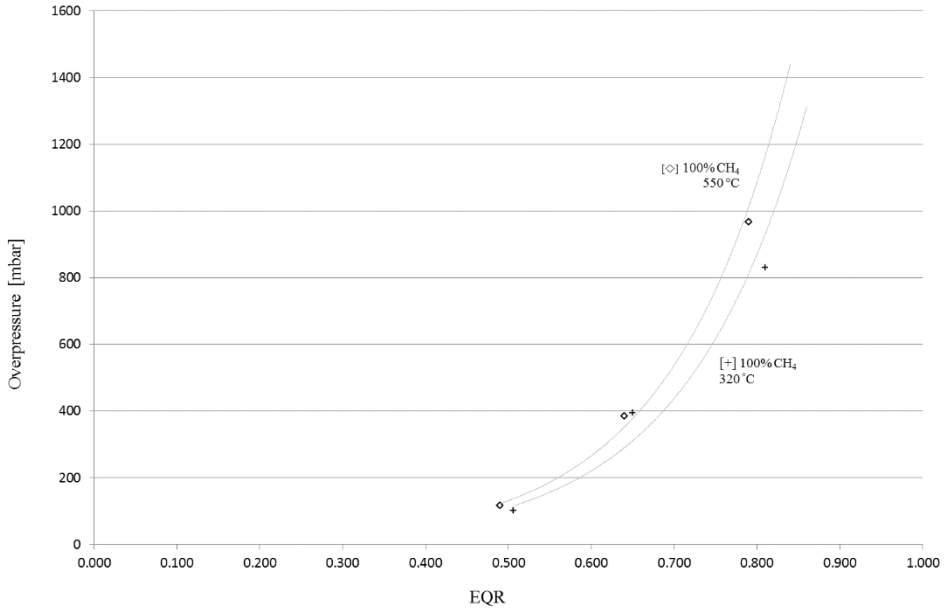

Figure 11. Peak pressure of explosion within the experimental rig plotted at different equivalence ratios for tests on 100% methane at nominal temperatures of 320 °C and 550 °C

Table 4. Tests on 60% methane and 40% hydrogen

Eq. Ratio	Peak Pressure mbar	Initial Pressure after HE mbar	Nominal Temperature °C
0.590	488	262	550
0.710	1211	534	550
0.510	250	117	550
0.600	514	210	320
0.500	123	53	320
0.705	3105	760	320

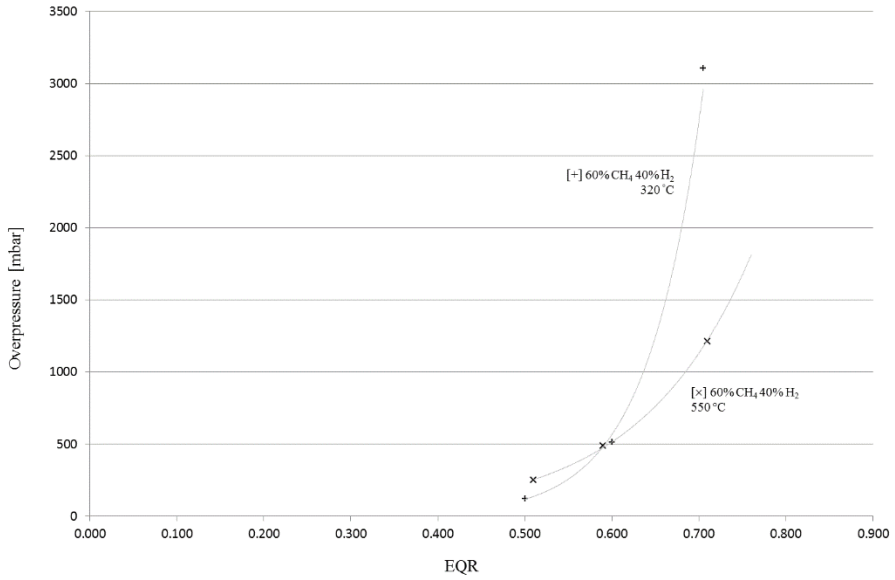

Figure 12. Peak pressure of explosion within the experimental rig plotted at different equivalence ratios for tests on 60% methane, 40% hydrogen at nominal temperatures of 320°C and 550°C

Table 5. Results of tests on 40% methane and 60% hydrogen

Eq. Ratio	Peak Pressure mbar	Initial Pressure after HE mbar	Nominal Temperature °C
0.550	776	390	550
0.620	1128	590	550
0.650	1753	1300	550
0.420	199	71	550
0.325	20	-	550
0.560	512	282	550
0.580	573	385	550
0.640	842	392	550
0.650	990	659	550
0.510	182	104	320
0.410	64	23	320
0.590	640	376	320

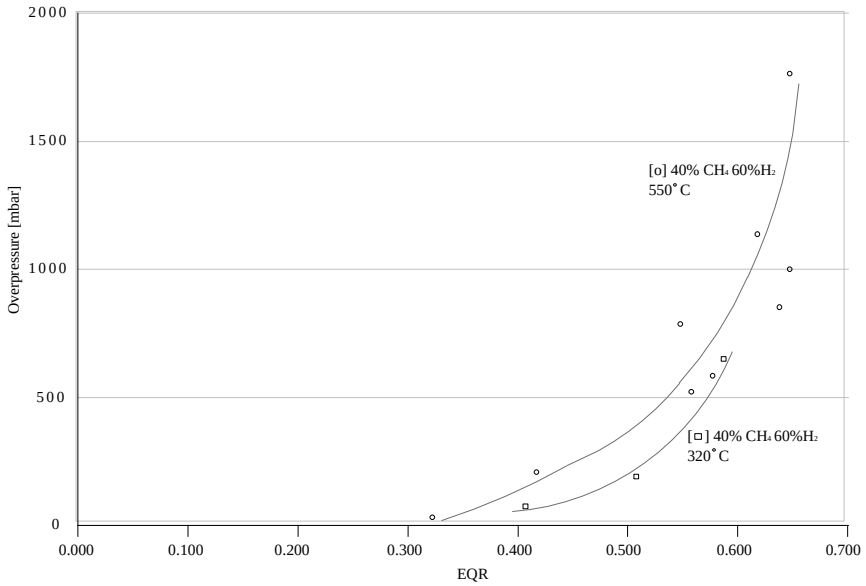

Figure 13. Peak pressure of explosion within the experimental rig plotted at different equivalence ratios for tests on 40% methane, 60% hydrogen at nominal temperatures of 320°C and 550°C

Table 6. Results of tests on 60% carbon monoxide with 40% hydrogen, and 100% hydrogen

Eq. Ratio	60%CO/40%H_2		40%CO/60%H_2		100% H_2		Nominal Temperature °C
	Peak Pressure mbar	Initial Pressure after HE mbar	Peak Pressure mbar	Initial Pressure after HE mbar	Peak Pressure mbar	Initial Pressure after HE mbar	
0.513			18228	6496			320
0.393			892	481			320
0.352			496	320			320
0.303			292	148			320
0.438	2688	1412					320
0.397	1009	433					320
0.323	315	135					320
0.450					2818	1487	320
0.350					0.500	267	320
0.285					0.159	140	320

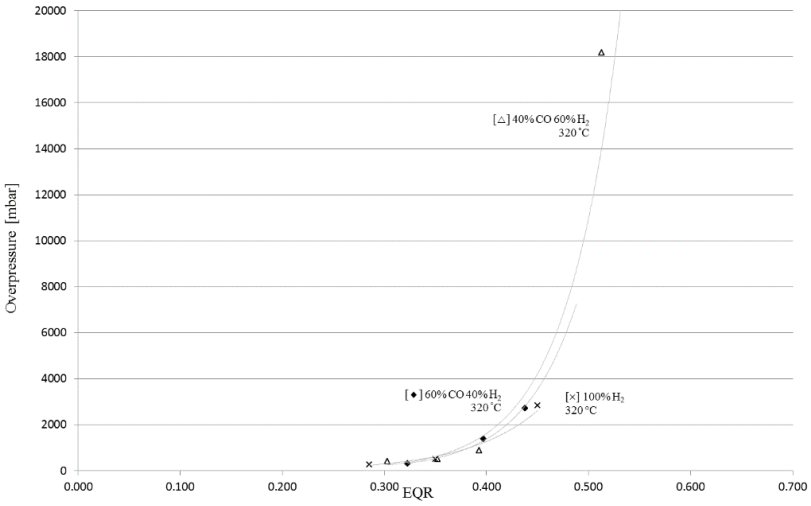

Figure 14. Peak pressure of explosion within the experimental rig plotted at different equivalence ratios for tests on 100%H_2; 60%H_2/40% CO and 40%H_2/60%CO at a nominal temperature of 320°C.

Discussion

In this section the common features across both the high and low temperature tests are discussed, in particular the pressure behaviour and flame speeds. Analysis of flame passage data such as shown in Figure 5 confirms the origin of the main source of transient pressure within the system. In addition, the monitoring of flame passage has allowed approximate flame velocities to be determined throughout the system. This data is more difficult to interpret since the flow behaviour within the HRSG is complex due to the vertical asymmetry and large separation zone in the expansion section. In general, the higher peak pressures are associated with higher measured flame speeds both upstream of the heat exchanger and in the immediate downstream region. Flame speeds at the circular duct exit can be as high as 330 m/s and around 250 m/s at the heat exchanger.

It has been emphasised that the origin of the pulse half width lies in the rate of combustion in the immediate heat exchanger downstream region and this is a region which is monitored by the downstream high-speed video camera which records the emergence of flame from the tubes of the heat exchanger at a rate of between 2500 and 3000 frames per secons. This gives a sufficiently good resolution to evaluate the progress of the flame from its first appearance around the base of the heat exchanger tubes to around the top of the chamber. It is considered that this time period is that associated with most of the generation of pressure within the system and therefore is also intimately associated with the rate of turbulent combustion in this important region.

The extraction of data from the video record is illustrated in the two figures below for cases at an exhaust temperature of 550 °C. Figure 15 is a sequence of frames involving 100% H_2, an EQR of 0.540, and where the resulting peak pressure at the heat exchanger is 1638 mbar. In this case the flame progress time is around 1.6 msec. This is a short time period and the majority of such times are in the range of 3 - 10 msec. However some progress times can be as long as 30 msec, as the example in Figure 16 shows, corresponding to 40% CH_4/60% H_2 and EQR of 0.51. In this case the peak heat exchanger pressure is weak at 117 mbar.

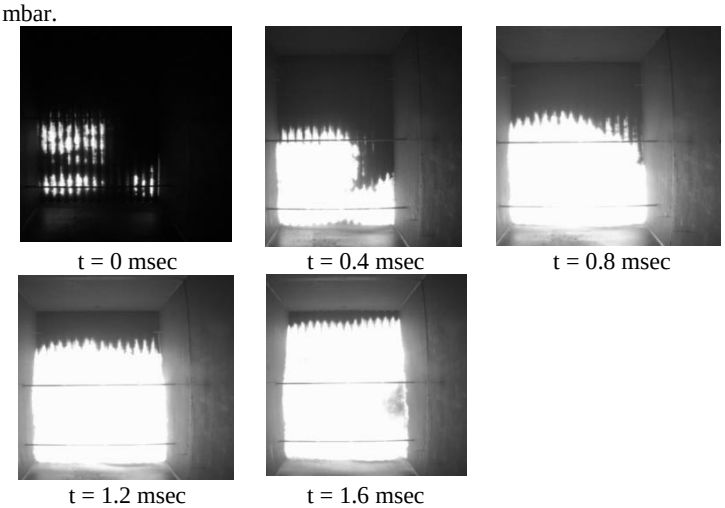

Figure 15. High speed video record from downstream looking at flame emergence from the heat exchanger. Fuel gas is 100% hydrogen and EQR of 0.540. Flame progression from the bottom to the top of the HRSG in around 1.6 msec.

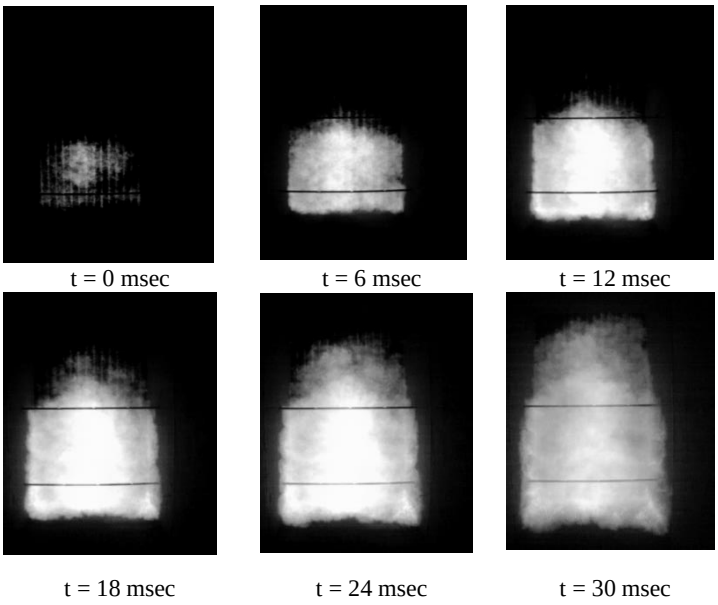

Figure 16. High speed video record from downstream looking at flame emergence from the heat exchanger. Fuel gas is 60% CH_4/40% H_2 at an EQR of 0.510. Flame progression from the bottom to the top of the HRSG in around 30 msec.

Figures 10 - 14 show consistent general behaviour, which demonstrates the sensitivity of peak pressure to change in both mixture composition and EQR value. In general, the higher intrinsic flame speed associated with hydrogen leads to higher peak pressures for the same EQR value compared with pure methane and correspondingly, the presence of methane in methane/hydrogen mixtures has a significant mitigating effect on pressure. The effect of reducing exhaust temperature has the effect of increasing the peak pressures observed for the case of pure hydrogen but the effect on other mixtures has been seen to be more variable. Of particular significance is the sensitivity of peak pressure to small changes in EQR value above certain threshold values. For example using a 60%CH_4/40%H_2 mixture at 550ºC, the peak pressure rises from 500 mbar to 3000 mbar between an EQR value of 0.6 and 0.7. This sensitivity behaviour is even more marked with pure hydrogen and indicates that control of fuel air mixture is critical to maintaining safe operating conditions in the event of a flameout.

Auto ignition and detonation behaviour

The behaviour of mixtures of hydrogen and carbon monoxide has shown characteristics which deserve a special mention. Preliminary studies for this work had shown that CO/H_2 mixtures demonstrated reactivity similar to pure hydrogen, and the results at 320 °C, shown in Figure 14, indicate that the peak pressures for pure H_2 at EQR values below 0.45 are similar to those of CO/H_2 mixtures. During the present set of tests it was noted that pre-ignition of the mixture very soon after fuel mixture injection was a recurrent problem and this ignition was identified as occurring around the heat exchanger tubes.

A high speed video camera located upstream of the heat exchanger and looking downstream into the heat exchanger tubes reveals the emergence of this flame kernel. For a normal ignition event, this flame progress is first seen as a fully formed flame progressing toward the heat exchanger tubes from the upstream circular duct exit. The pre-ignition event sequence is shown in Figure 17 and reveals the reverse sequence of flame progress. It is noted that for these events to occur, the surface temperature of the tubes would be expected to be close to the exhaust temperature at that point, i.e. 300 - 400ºC.

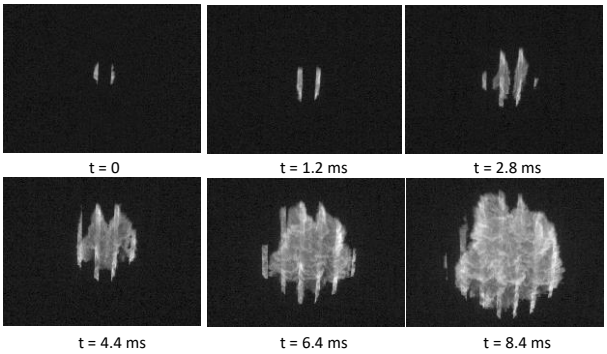

Figure 17. Frame sequence from upstream high-speed camera showing the progress of flame following a pre-ignition event using 60%CO/40%H_2. (This record confirms that ignition originates within finned tube array, with flame progressing back upstream between t=0 and t= 8.4 msec.)

Figure 14 also reveals that a single test case gave rise to a detonation event corresponding to an EQR of 0.513 using 60%H_2/40% CO. For comparison with Figure 15, the bottom - top flame transit time for this detonation case this was 0.8 msec. An estimation of the flame speeds from the flame sensors within the HRSG section are close to 2000 m/s, which is consistent with development of a detonation event occurring in the region between the heat exchanger and the end plate.
In addition, an examination of the flame arrival and pressure wave arrival data downstream of the heat exchanger indicates that the pressure wave and flame front are almost coincident, i.e. consistent with the passage of a detonation wave. This event was not anticipated and underlines the sensitivity of the combustion rate with EQR. In this case an EQR change from 0.40 - 0.51 raised the peak pressure from 1000 mbar to 18228 mbar.

Conclusions

The large body of results have enabled estimates to be made of the likely peak pressure likely to arise from using particular mixtures as a function of EQR values. Given that limits on pressure tolerance of large HRSG structures are around 0.3 barg, this data can be used to judge the limiting conditions of EQR which might safely be used for different mixtures and at different exhaust temperatures. The graphs shown have enabled a table of safe operating conditions to be developed and this is shown in Table 7 below. The analytical curve fits for each graph, however, allow other tolerance criteria to be established.

Table 7. Summary of EQR limit values based on HR4 peak pressures of 0.3 barg

Mixture, %	Exhaust Temperature	EQR limit value
100 CH_4	HIGH	0.7
	LOW	0.77
100 H_2	HIGH	0.43
	LOW	0.36
60 CH_4 / 40 H_2	HIGH	0.63
	LOW	0.63
40 CH_4 / 60 H_2	HIGH	0.57
	LOW	0.57
60 CO / 40 H_2	HIGH	0.39
	LOW	0.38
40 CO / 60 H_2	HIGH	-
	LOW	0.35

The broad conclusions to be drawn from the graphs presented can be summarised as follows:

1. Methane is the least reactive of the group, allowing the greatest EQR values to be used.
2. Increasing the hydrogen content in the methane mixture will increase the reactivity and reduce the value of any EQR limit value based on a chosen maximum explosion peak pressure level.
3. Carbon monoxide/hydrogen mixtures behave in a very similar way with respect to their contribution to the reactivity of the mixtures. In this regard 40%H2/60%CO mixtures behave in a closely similar way to 60%H2/40%CO mixtures. This is confirmed by the similar EQR limit values in Table 7, particularly for the low temperature cases, where the data is more complete.
4. Carbon monoxide/hydrogen mixtures behave in a similar way to pure hydrogen - again the low temperature EQR limit values provide an indication of this.
5. Methane provides a mitigating effect on the rate of combustion and therefore on the peak pressures developed. This is confirmed from the behaviour of other studies using the 25%CH_4/35%CO/40%H_2 mixture and one must assume from Table 7, that as the methane content varies from 25% to 100%, the EQR limit value will vary from the indicated value of 0.77 at low temperature to around 0.35 for a CO/H_2 mixture.

References

Arntzen, B.J., Hjertager, B., Lindstedt, R.P., Mercx, W.P.M. and Popat, N., (1995) Investigations to Improve and Assess the Accuracy of Computational Fluid Dynamic Based Explosion Models, *Journal of Hazardous Materials*, 45:1-25.

BS-EN-1127. (2011). *Explosive atmospheres - Explosion prevention and protection - Part 1: Basic concepts and methodology.*

BS-ISO-21789. (2009). *Gas turbine applications - Safety.*

Gamezo, V.N., Ogawa, T. & Oran, E.S. (2007) Numerical simulations of flame propagation and DDT in obstructed channels filled with hydrogen–air mixture, *Proceedings of the Combustion Institute* 31: 2463-2471.

International Electrotechnical Commission, Electrical apparatus for explosive gas atmospheres - Part 20: Data for flammable gases and vapours, relating to the use of electrical apparatus, Standard IEC 60079-20:2000

ISO-PDTR-15916. (2010). *Basic considerations for the safety of hydrogen systems.*

Kuan T.S., Lindstedt, R.P. and Vaos, E.M., (2003) Higher Moment Based Modeling of Turbulence Enhanced Explosion Kernels in Confined Fuel-Air Mixtures, Advances in Confined Detonations and Pulse Detonation Engines, ISBN 5-94588-012-4, Torus Press, pp. 17-40.

Lindstedt, R.P. and McCann, H.A. (2001) Time Resolved Flow Characteristics of Confined Turbulent Gaseous Explosions. Presented at 18th ICDERS, Seattle.

National Aeronautics and Space Administration Report, Safety Standard for Hydrogen and Hydrogen Systems, Report NSS 1740.16, 1997, p. A-16.

NFPA-68. (2008). *Standard on explosion prevention systems.*

NFPA-85. (2011). *Boiler and combustion systems hazards code.*

IGEM-UP-3. (2006). *Gas fuelled spark ignition and dual fuel engines.* The Institute of Gas Engineers and Managers, UK.

Santon, R. (2005). A Review of UK Onshore and Offshore Installations. *Institution of Diesel and Gas Turbine Engineers.*